Raman scattering in a nearly resonant density ripple

Hugh C. Barr[a] and Francis F. Chen
Department of Electrical Engineering, University of California, Los Angeles, California 90024

(Received 20 August 1986; accepted 10 December 1986)

Stimulated Raman scattering of light waves by an underdense plasma is affected by the presence of a density ripple caused by a simultaneously occurring stimulated Brillouin instability. The problem is treated kinetically for the particularly interesting case where the ripple has nearly the same wavelength as the plasma wave. The ripple is found to reduce the growth rate of the usual Raman instability but allows other decay modes to occur. Numerical results for the frequencies, growth rates, and k spectra of these modes are obtained. A physical explanation is given for a baffling result of the calculation. The physical picture is also of interest to particle acceleration by plasma waves.

I. INTRODUCTION

The stimulated Raman scattering (SRS) instability, in which a light wave decays into a red-shifted light wave and an electron plasma wave, has been under intense study[1] because of its potential for fuel preheat in laser fusion targets. Indeed, SRS has been identified in solid–target experiments with both 1 and 0.5 μm light,[2] and even with wavelengths as short as 0.35 μm.[3] Since the threshold for exciting ion acoustic waves via stimulated Brillouin scattering (SBS) is generally lower than for SRS, the interference between these instabilities can alter their thresholds. The presence of SBS during SRS experiments has been confirmed by several groups using underdense plasma targets.[4–6] In a more recent application, laser excitation of plasma waves has been proposed as a new way to make particle accelerators.[7] In experiments testing this concept,[8] SRS and SBS are both found to occur.

Since a plasma wave is sensitive to density variations, which change the plasma frequency $\omega_p = (4\pi n_0 e^2/m)^{1/2}$, the existence of a density ripple in the form of an ion wave excited by SBS could greatly affect the SRS mechanism. One can foresee two competing effects: (1) The density modulation could generate shorter wavelength harmonics, which lead to enhanced Landau damping; and (2) the partial or complete reflection of plasma waves at the density maxima could lead to decreased convective losses or absolute instability. We shall find that both of these effects occur and are linked in a complicated way.

Let the undepleted pump wave $(\omega_0, \mathbf{k}_0)$ be of the form $\mathbf{E} = 2\mathbf{E}_0 \cos(k_0 - \omega_0 t)$ and decay into a scattered wave $(\omega_s, \mathbf{k}_s)$ and a plasma wave $(\omega, \mathbf{k})$ that follow the respective dispersion relations

$$\omega_s = \omega_p^2(x) + k_s^2 c^2, \tag{1}$$

$$\omega^2 = \omega_p^2(x) + 3k^2 v_e^2, \tag{2}$$

and the ω- and k-matching conditions

$$\omega_0 = \omega_s + \omega, \quad \mathbf{k}_0 = \mathbf{k}_s + \mathbf{k}, \tag{3}$$

where $v_e^2 = KT_e/m = \lambda_D^2 \omega_p^2$. We neglect pump depletion and assume $\omega_p \ll \omega_0$, so that Eqs. (1)–(3) imply that $k \cong 2k_0$ for direct backscattering, and that the variation in k_s can be neglected. Let the density be simusoidally modulated so that

$$\omega_p^2(x) = \omega_{p0}^2(1 + \epsilon \cos k'x). \tag{4}$$

Consider first the case where the ripple is caused by the plasma production process; for instance, by gaps in the magnetic field coils. Then $k' \ll k$ and $k(x)$ changes slowly inside the ripple. If $\epsilon < 3k_D^2 \lambda_D^2$, the thermal term in Eq. (2) can accommodate the change in ω_p^2 by a variation in k. The plasma wave becomes nonsinusoidal and develops spatial harmonics that change the Landau damping. If $\epsilon > 3k_0^2 \lambda_D^2$, on the other hand, Eq. (2) requires k to become imaginary at the density maxima, and the plasma wave will be trapped in the density troughs. Moreover, the wave is not excited over the entire trapping distance. In a plasma with a parabolic profile $n_0 \propto 1 \pm x^2/L_n^2$, for instance, the phase mismatch caused by a change in k in Eq. (3) grows to the order of π in a distance[9] $L_1 \cong (18k\lambda_D^2 L_n^2)^{1/3}$, while the wave is trapped in a length $L_2 \cong 12^{1/2} k\lambda_D L_n$. Thus the ratio L_1/L_2 is $\cong (k^2 \lambda_D L_n)^{-1/3}$, which is usually small ($\cong 10\%$ for $L_n = 1$–10 cm and unrippled $k\lambda_D \cong 0.1$). The wave is excited only near the density minima and coasts to its reflection point. This physical situation could lead to absolute instability, but of a different nature from those previously considered, where the trapping of wave energy comes from partial reflection at plasma boundaries.[10]

This paper, however, emphasizes the special case $k' \cong k$, since the SBS ion wave and the SRS plasma wave both have $k \cong 2k_0$ in underdense backscattering. Specifically, we may neglect the difference between k' and $2k_0$ (because the ion wave is of such low frequency) and calculate k from Eqs. (1)–(3), obtaining

$$k - 2k_0 \cong -\omega_p/c = -k_0(n/n_c)^{1/2}. \tag{5}$$

The wavenumber difference is small but essential. Since the plasma wave has nearly the same wavelength as the density ripple, spatial harmonics are readily excited, and there is considerable tunneling through the reflection points even if ϵ is large. Similar problems have been treated previously by several authors. Kaw, Lin, and Dawson[11] were the first to treat the mode-coupling problem in this connection; they used a fluid formulation and did not consider the effect of a pump. Nicholson[12] also employed a fluid treatment but assumed that the group velocity directions were given, thus leaving out mode coupling. Rozmus *et al.*[13] treated the prob-

[a] Permanent address: University College of North Wales, University of Wales, Bangor LL57 2UW, Wales.

 0031-9171/87/041180-09$01.90

lem kinetically, but in emphasizing turbulent rather than coherent fluctuations did not consider the interesting mode-coupling effects discussed here.

We first give a fluid treatment in order to bring out the physical effects; then, in Sec. III, we give the kinetic formulation on which the computations are based. The final sections concern the physical interpretation of the results.

II. FLUID THEORY

The coupled mode equations describing stimulated Raman scattering in one dimension are[14]

$$\left(\frac{\partial^2}{\partial t^2}+\omega_p^2(x)-3v_e^2\frac{\partial^2}{\partial x^2}\right)n_1=n_0\frac{\partial^2}{\partial x^2}(v_0v_s), \tag{6}$$

$$\left(\frac{\partial^2}{\partial t^2}+\omega_p^2(x)-c^2\frac{\partial^2}{\partial x^2}\right)v_s=-v_0\omega_p^2n_1/n_0, \tag{7}$$

where v_0 and v_s are the quiver velocities $v_{0,s}=eE_{0,s}/m\omega_{0,s}$ in the pump and scattered waves, respectively; n_1 is the density perturbation of the plasma wave; and ω_p^2 is the square of the spatially varying plasma frequency, $\omega_p^2(x)=4\pi e^2n_0(x)/m$. We consider a density ripple of the form

$$n_0(x)=N_0(1+\epsilon\cos 2k_0x). \tag{8}$$

Assuming $n_1\propto\exp(-i\omega t)$ and $v_s\propto\exp i(k_sx-\omega_st)$ and neglecting the variation of ω_p in Eq. (7), we may solve Eq. (7) for v_s and substitute into Eq. (6), keeping only the low-frequency part of v_0v_s. The result is Mathieu's equation

$$\frac{d^2y}{dz^2}+(a-2q\cos 2z)y=0, \tag{9}$$

where

$$z\equiv k_0x,\quad y\equiv n_1/N_0, \tag{10}$$

$$a\equiv(\omega^2-\omega_p^2)/(3k_0^2v_e^2+\Delta^2), \tag{11}$$

$$q\equiv(\epsilon\omega_p^2/2)/(3k_0^2v_e^2+\Delta^2), \tag{12}$$

$$\Delta^2\equiv(k_0^2v_0^2\omega_p^2)/(\omega_s^2-\omega_p^2-k_s^2c^2), \tag{13}$$

$$\omega_p^2\equiv 4\pi e^2N_0/m. \tag{14}$$

The quantity Δ is a small frequency shift as a result of ponderomotive force; except for this, Eqs. (9)–(14) are the same as what Kaw *et al.*[11] previously analyzed. The parameter q separates the cases of wave trapping or no wave trapping, as explained in Sec. I, the critical ripple size being given by $q=1$ when $\Delta=0$.

In an infinite plasma, the solutions of Eq. (9) must have the same period as cos 2z, and the conditions for periodicity determine the eigenvalues $a(q)$, which specify the eigenfrequencies ω. The standard solutions, or Mathieu functions,[15] have series expressions for either large q or small q, and the behavior for intermediate q has been studied numerically. The physical situation is simpler than the mathematical one. When q is small, the spatial harmonics are weakly coupled, and the series can obviously be truncated. When q is large, an infinite number of harmonics can be important in principle, but in practice a natural truncation occurs because of Landau damping.

The nature of plasma waves in a rippled medium can be seen by considering the undriven case $\Delta=0$ in the limit $q\ll 1$, or $\epsilon\ll 6k_0^2\lambda_D^2$. Let

$$y=\sum_\kappa y_\kappa e^{i(\kappa z-\omega t)} \tag{15}$$

and substitute into Eq. (9). Equating the coefficients of terms with the same periodicity yields the recursion relation

$$(a-\kappa^2)y_\kappa=q(y_{\kappa-2}+y_{\kappa+2}) \tag{16}$$

for the Fourier amplitudes y_κ. Since $k\cong 2k_0$ for the SRS-driven waves, the uncoupled value of κ is $\cong 2$ and of a is $\cong 4$. More exactly, let the driven mode have $\kappa=\bar\kappa\equiv 2-\delta$, where, from Eq. (5),

$$\delta=\omega_p/ck_0\ll 2. \tag{17}$$

This "red shift" is caused by the frequency difference between the SRS-driven plasma waves and the SBS-driven ion waves. Successively setting κ equal to $\bar\kappa-2$, $\bar\kappa$, $\bar\kappa-4$, $\bar\kappa+2$, and $\bar\kappa-6$ (or $\kappa\cong 0,\pm 2,\pm 4$) in Eq. (16), we obtain a set of five simultaneous equations

$$(a-\underline{\delta^2})y_0=q(y_2+y_{-2}), \tag{18}$$

$$[a-(2-\delta)^2]y_2=q(y_0+y_4), \tag{19}$$

$$[a-(2+\delta)^2]y_{-2}=q(y_0+y_{-4}), \tag{20}$$

$$[a-(4-\underline{\delta})^2]y_4=q(y_2+y_6), \tag{21}$$

$$[a-(4+\underline{\delta})^2]y_{-4}=q(y_{-2}+y_{-6}). \tag{22}$$

We truncate by setting $y_{\pm 6}=0$, thus closing the system, and further neglect the underlined terms $\underline{\delta}$, since $a\cong 4$. The system becomes

$$ay_0=q(y_2+y_{-2}), \tag{23}$$

$$[a-(2-\delta)^2]y_2=q(y_0+y_4), \tag{24}$$

$$[a-(2+\delta)^2]y_{-2}=q(y_0+y_{-4}), \tag{25}$$

$$(a-16)y_4=qy_2, \tag{26}$$

$$(a-16)y_{-4}=qy_{-2}. \tag{27}$$

First, consider the case of a resonant ripple, $\delta=0$. The determinantal equation that ensures the solubility of this set of five homogeneous equations yields a fifth-order equation for $a(q)$:

$$[(a-4)(a-16)-q^2][a(a-4)(a-16)-q^2(3a-32)]=0. \tag{28}$$

By substituting $y_2=\pm y_{-2}$ into Eqs. (23)–(27), it is easily seen that the vanishing of the first and second brackets in Eq. (28) corresponds to odd ($y_2=-y_{-2}$, $y_0=0$) and even ($y_2=y_{-2}$, $y_0\neq 0$) solutions, respectively. Since q^2 is small, odd solutions occur for $a\cong 4$ and $a\cong 16$. The eigenvalue of importance to us is $a\cong 4$:

$$(\mathrm{se}_2):\ a=4-q^2/12\quad(\omega=\omega_1). \tag{29}$$

This is recognized as the value of a, correct to order q^2, for the Mathieu function $\mathrm{se}_2=\sin 2z-(q/12)\sin 4z+\cdots$. From the second bracket, we see that even solutions occur for $a=0$, 4, and 16. The eigenvalue near $a=4$ is

$$(\mathrm{ce}_2):\ a=4+\tfrac{5}{12}q^2\quad(\omega=\omega_2), \tag{30}$$

which corresponds to the Mathieu function

$$\mathrm{ce}_2=\cos 2z-(q/12)(\cos 4z-3)+\cdots.$$

The eigenvalue near $a=0$ will also be of importance to us:

$$(\mathrm{ce}_0):\ a=-\tfrac{1}{2}q^2\quad(\omega=\omega_3). \tag{31}$$

Thus, we see that the ripple splits the original frequency into one (ω_1) which is lower, and another (ω_2) which is higher; and in addition introduces a new low frequency (ω_3), as well as harmonics with $a \cong 16$, which are not as important.

We now consider a ripple that is nearly resonant with the plasma wavelength but not exactly so. Equations (23)–(27) are to be solved with $0 < |\delta| \ll 2$. Eliminating $y_{\pm 4}$ and y_0 and letting $a \cong 4$ in small terms containing q^2, we obtain two equations for y_2 and y_{-2}, whose determinant yields

$$\left(a - (2-\delta)^2 - \frac{q^2}{6}\right)\left(a - (2+\delta)^2 - \frac{q^2}{6}\right) = \frac{q^4}{16}. \tag{32}$$

With the definition

$$R \equiv q^2/16\delta, \tag{33}$$

the solutions to Eq. (32) can be written simply as

$$a_\pm = 4 + \delta^2 + q^2/6 \pm 4\delta(1+R^2)^{1/2}. \tag{34}$$

These eigenvalues correspond to $\omega = \omega_2$ and $\omega = \omega_1$; ω_3 has been neglected in taking $a \cong 4$. The actual frequencies are found from Eq. (11):

$$\omega_{2,1}^2 = \omega_p^2 + 3k_0^2 v_e^2 a_\pm. \tag{35}$$

The frequency splitting apparently depends on the ratio R between the effects of ripple size and wavelength mismatch. To estimate this ratio for $\Delta = 0$, we find from Eqs. (12) and (17)

$$q = (\epsilon/6)(c^2/v_e^2)(n/n_c), \tag{36}$$

$$R = (q^2/16)(n_c/n)^{1/2}. \tag{37}$$

For typical gas-target experiments where $n/n_c \cong v_e/c \cong \epsilon \cong 10^{-2}$, we have $q \cong 0.17$ and $R \cong 0.017$, so that both q^2 and R are small. For solid-target experiments, however, typical values are $n/n_c \cong \epsilon \cong 10^{-1}$, $v_e/c \cong 0.03$, giving $q = 1.85$ and $R = 0.68$. In this case q and R are so large that numerical solution is required.

For later use in Sec. IV, we compute the Fourier amplitudes $y_{\pm 2}$ for the eigenmodes ω_1 and ω_2. Eliminating $y_{\pm 4}$ from Eqs. (23)–(27) yields

$$\begin{aligned} q y_0 &= \{a - (2-\delta)^2 + q^2/12\} y_2 \\ &= \{a - (2+\delta)^2 + q^2/12\} y_{-2}. \end{aligned} \tag{38}$$

Substituting a from Eq. (34) gives

$$\frac{y_{-2}}{y_2} = 1 \pm \frac{(1+R^2)^{1/2}}{R} \begin{Bmatrix} \omega_1 \\ \omega_2 \end{Bmatrix}. \tag{39}$$

For sufficiently large ripple, R is $\gg 1$ and $y_{-2} = \pm y_2$; we have standing waves as expected. However, if R is small, Eq. (39) gives

$$\frac{y_{-2}}{y_2} \cong \begin{Bmatrix} -R/2 \\ +2/R \end{Bmatrix} \begin{Bmatrix} \omega_1 \\ \omega_2 \end{Bmatrix}, \tag{40}$$

which shows that the normal modes are primarily traveling waves. In SRS, y_2 is the driven component at $k \cong 2k_0$, while y_{-2} is a backward wave with $k \cong -2k_0$ excited by mode coupling through the idler at $k \cong 0$. For small R, Eq. (40) shows that the lower-frequency root ω_1 has $|y_{-2}| \ll |y_2|$, so that it appears to be the original plasma wave, modified by the ripple. The higher-frequency root ω_2, on the other hand, has $|y_{-2}| \gg |y_2|$, and so must be a new wave excited only in the presence of a ripple.

That the higher-frequency mode ω_2 should always be traveling in the $-\mathbf{k}_0$ direction seems unreasonable, since the excitation term Δ has been neglected in the derivation of Eq. (40), and we could have considered y_{-2} to be the driven component. Symmetry is restored when we consider that δ was implicitly taken as positive, meaning that the driven mode has a $|k|$ smaller than $|2k_0|$. If the sign of δ is reversed, we see from Eqs. (23)–(27) that the roles of y_2 and y_{-2} would also be reversed. Thus, whether the new mode that arises from mode coupling has higher or lower frequency than the driven wave depends on whether the driven wave has longer or shorter wavelength than the ripple.

We next add the ponderomotive drive Δ^2 to calculate the growth rates. Equation (32) is correct whether or not the quantity a is defined with a term Δ^2. In adding Δ^2, however, we must not add it to all members of the set of Eqs. (23)–(27), but only to the equation for the mode that is resonant with the drive. If we assume that SRS is set up to drive only the mode $\mathbf{k} \cong +2\mathbf{k}_0$, then Δ^2 should appear in the definition of a and q only in Eq. (24). Equation (32) is then modified to read

$$\left(a_1 - (2-\delta)^2 - \frac{qq_1}{6}\right)\left(a - (2+\delta)^2 - \frac{q^2}{6}\right) - \frac{q^3 q_1}{16} = 0, \tag{41}$$

where

$$\begin{aligned} a &= \frac{\omega^2 - \omega_p^2}{3k_0^2 v_e^2}, \quad q = \frac{\epsilon \omega_p^2}{6k_0^2 v_e^2}, \\ \begin{Bmatrix} a_1 \\ q_1 \end{Bmatrix} &= \begin{Bmatrix} a \\ q \end{Bmatrix} \left(1 + \frac{\Delta^2}{3k_0^2 v_e^2}\right)^{-1}. \end{aligned} \tag{42}$$

Using Eq. (13), we can write a_1 and q_1 as

$$a_1 = a/(1+d), \quad q_1 = q/(1+d), \tag{43}$$

where, for $d \ll 1$,

$$d \cong \frac{1}{3}\frac{v_0^2}{v_e^2}\frac{\omega_p^2}{\omega_s^2 - \omega_p^2 - k_s^2 c^2}. \tag{44}$$

Since this term will make ω complex, let

$$\omega_\pm = \omega_{2,1} + i\gamma_\pm. \tag{45}$$

SRS can now drive either of these modes, giving two scattered frequencies ω_s:

$$\omega_s = \omega_0 - \omega_\pm = \omega_0 - \omega_{2,1} - i\gamma_\pm. \tag{46}$$

Assuming that the real part of ω_s is frequency matched, we obtain

$$d = \frac{i}{6}\frac{v_0^2}{v_e^2}\frac{\omega_p^2}{\omega_0 \gamma_\pm}. \tag{47}$$

Since $\omega_{1,2}$ are the roots of Eq. (32), that equation can be written

$$(3k_0^2 v_e^2)^{-2}(\omega^2 - \omega_1^2)(\omega^2 - \omega_2^2) = 0. \tag{48}$$

Equation (41) is the same equation with an added term in d, so it can be written

$$\begin{aligned} &(3k_0^2 v_e^2)^{-2}(\omega^2 - \omega_1^2)(\omega^2 - \omega_2^2) - d(2-\delta)^2 \\ &\quad \times [a - (2+\delta)^2 - q^2/6] = 0. \end{aligned} \tag{49}$$

Replacing a by the expression in Eq. (34) and combining with Eq. (47) for d, we obtain

$$(\omega^2-\omega_2^2)(\omega^2-\omega_1^2)=24i(k_0^2v_e^2)(k_0^2v_0^2)(\omega_p^2\delta/\omega_0\gamma_\pm)\times[-1\pm(1+R^2)^{1/2}]. \quad (50)$$

For the root $\omega\cong\omega_2$, we take the $+$ signs, and the left-hand side becomes $\cong -2i\omega_2\gamma_+(\omega_2^2-\omega_1^2)$. Equations (34) and (35) give

$$\omega_2^2-\omega_1^2=3k_0^2v_e^2\cdot 8\delta(1+R^2)^{1/2}. \quad (51)$$

Inserting into Eq. (50), we obtain

$$(\omega_2):\ \gamma_+^2=\tfrac{1}{2}\gamma_0^2[1-(1+R^2)^{-1/2}], \quad (52)$$

where

$$\gamma_0\equiv(v_0/c)(\omega_0\omega_p)^{1/2} \quad (53)$$

is the SRS homogeneous growth rate in the absence of ripple.[14] Similarly, for the $\omega\cong\omega_1$ mode we obtain

$$(\omega_1):\ \gamma_-^2=\tfrac{1}{2}\gamma_0^2[1+(1+R^2)]^{-1/2}. \quad (54)$$

Thus, as the ripple size q, and hence R, is reduced, the original mode ω_1 grows at the usual rate γ_0, while the ripple-generated mode ω_2 approaches zero growth rate. When R is sufficiently large, both modes grow at the same rate $\gamma=\gamma_0/\sqrt{2}$.

To solve for the growth rate of the mode $\omega_3(a\cong 0)$, we must go back to Eqs. (18)–(22), which do not assume $a\cong 4$. For this mode, we may neglect $y_{\pm 4}$ and also δ relative to 2. Equations (18)–(20) then give

$$(a-\delta^2)y_0=q(y_2+y_{-2}), \quad (55)$$

$$(a_1-4)y_2=q_1y_0,\quad (a-4)y_{-2}=qy_0, \quad (56)$$

where a_1 and a are given by Eq. (42) if the pump is still k matched to the $\mathbf{k}\cong 2\mathbf{k}_0$ mode. These give

$$a=\delta^2+q[q_1/(a_1-4)+q/(a-4)]. \quad (57)$$

When there is no pump, we may set $a_1=a\cong 0$ and obtain

$$a=\delta^2-\tfrac{1}{2}q^2 \quad (58)$$

in agreement with Eq. (31) for $\delta=0$. The frequency is therefore given by

$$\omega_3^2=\omega_p^2+3k_0^2v_e^2(\delta^2-\tfrac{1}{2}q^2). \quad (59)$$

In the presence of excitation, we assume that a scattered frequency $\omega_s=\omega_0-\omega_3$ is produced, whereupon Eqs. (43) and (47) for d are still valid. Using this in Eq. (57) and proceeding as before, we obtain

$$\gamma_3=(q/4)\gamma_0. \quad (60)$$

This mode has a smaller intrinsic growth rate than ω_1 or ω_2 but may be important when damping is included because of the lack of Landau damping on such a long-wavelength mode.

III. KINETIC CALCULATIONS

To treat the natural truncation of the system of harmonics, we now reformulate the problem kinetically to include Landau damping. The electrons are described by Vlasov's equation

$$\frac{\partial f}{\partial t}+v\frac{\partial f}{\partial x}-\left(\frac{e}{m}E(x,t)+\frac{1}{m}\frac{\partial\psi(x,t)}{\partial x}\right)\frac{\partial f}{\partial v}=0, \quad (61)$$

where $f=f(x,v,t)$ is the one-dimensional electron distribution function and $\psi(x,t)$ is the ponderomotive potential. The equilibrium distribution is taken to be

$$f_0(x,v)=n_0(x)F_M(v), \quad (62)$$

where $F_M(v)$ is a Maxwellian, and $n_0(x)$ is given by Eq. (8). The small electric field of the ion wave is small and static and can be ignored. Linearization of Eq. (61) yields

$$\frac{\partial f_1}{\partial t}+v\frac{\partial f_1}{\partial x}=\left(\frac{e}{m}E+\frac{1}{m}\frac{\partial\psi}{\partial x}\right)F_M'(v)n_0(x). \quad (63)$$

Fourier analyzing in time and space, we obtain

$$f_1(k,v,\omega)=[ieN_0/m(\omega-kv)]F_M'(v)[a(k,\omega)+\tfrac{1}{2}\epsilon a(k+2k_0,\omega)+\tfrac{1}{2}\epsilon a(k-2k_0,\omega)], \quad (64)$$

where

$$a(k,\omega)\equiv(e/m)E(k,\omega)+(ik/m)\psi(k,\omega). \quad (65)$$

Integration over v yields

$$n_1(k,\omega)=(ik/4\pi e)\chi(k,\omega)[a(k,\omega)+\tfrac{1}{2}\epsilon a(k+2k_0,\omega)+\tfrac{1}{2}\epsilon a(k-2k_0,\omega)], \quad (66)$$

where $\chi(k,\omega)$ is the usual electron susceptibility

$$\chi(k,\omega)=-\frac{\omega_p^2}{k^2}\int dv\frac{F_M'(v)}{v-\omega/k}=-\frac{1}{2k^2\lambda_D^2}Z'(\zeta). \quad (67)$$

Here $Z(\zeta)$ is the Fried–Conte function[16] and ζ is $\omega/kv_e\sqrt{2}$. Combining Eq. (66) with Poisson's equation, we obtain

$$[1+1/\chi(k,\omega)]E(k,\omega)+(ik/e)\chi(k,\omega)=(\epsilon/2)[E(k+2k_0,\omega)+E(k-2k_0,\omega)+(k+2k_0)(i/e)\psi(k+2k_0,\omega)+(k-2k_0)(i/e)\psi(k-2k_0,\omega)]. \quad (68)$$

The ponderomotive potential $\psi(k,\omega)$ at the plasma wave frequency arises from the beat between E_0 and E_s. We assume that these waves are not affected the ripple, since ω_p^2 is a small term in their dispersion relation, Eq. (1), as long as $n\ll n_c$. The scattered wave is described by Eq. (7), which can be written as

$$D(k_s,\omega_s)E(k_s,\omega_s)=-(\omega_p^2/N_0)n_1(k,\omega)E_0, \quad (69)$$

where

$$\mathbf{k}_s=\mathbf{k}-\mathbf{k}_0,\quad \omega_s=\omega-\omega_0,$$

and

$$D(k_s,\omega_s)=k_s^2c^2-\omega_s^2+\omega_p^2. \quad (70)$$

With an incident field $\mathbf{E}_0=2E\hat{\mathbf{x}}\cos(k_0x-\omega_0t)$, the ponderomotive potential can be written

$$\psi(k,\omega)=(e^2/m\omega_0^2)E_0E(k_s,\omega_s)=iev_0^2kE(k,\omega)/D(k_s,\omega_s). \quad (71)$$

Using this in Eq. (68), we finally obtain

$$\left(1+\frac{1}{\chi(k,\omega)}-\frac{k^2v_0^2}{D(k_s,\omega_s)}\right)E(k,\omega)=-\frac{\epsilon}{2}\left[E(k+2k_0,\omega)\left(1-\frac{(k+2k_0)^2v_0^2}{D(k+k_0,\omega-\omega_0)}\right)+E(k-2k_0,\omega)\left(1-\frac{(k-2k_0)^2v_0^2}{D(k-3k_0,\omega-\omega_0)}\right)\right]. \quad (72)$$

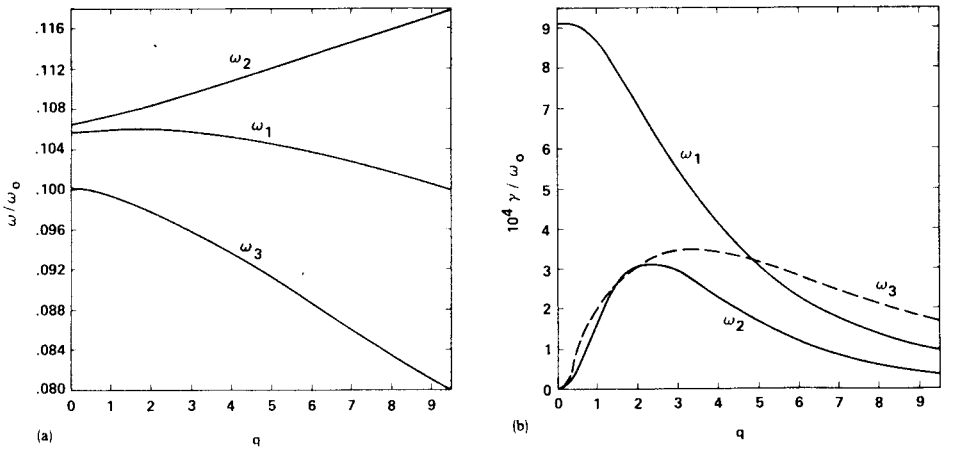

FIG. 1. (a) Frequencies ω and (b) growth rates γ of the original mode ω_1 and ripple-generated modes ω_2 and ω_3, as functions of ripple amplitude q.

This is the analog of the fluid equation (16) and is the primary result of this paper. It represents an infinite set of homogeneous difference equations whose solution yields an infinite set of eigenfrequencies. In practice, only a few members of this set are important. If ϵ is small, we can truncate as in Sec. II to obtain solutions correct to any specified power of q. If $q > 1$, mode coupling is strong, but a natural truncation occurs because large-k modes have $k\lambda_D > 1$ and are heavily damped. The pump-dependent terms on the right-hand side of Eq. (72) represent the beat of $\psi(k,\omega)$ with the ripple at $(0, 2k_0)$. They are significant only when the denominators are resonant, and they are small enough to be neglected even then, just as we neglected Δ^2 in Eq. (12) for q. As it stands, Eq. (72) describes both Raman backscattering ($k \cong 2k_0$) and forward scattering ($k \cong \omega_p/c$). The fluid equations of Sec. II can easily be recovered by expanding the Z function for $|\zeta| \gg 1$.

The system of Eqs. (72) has been solved numerically for parameters typical of a gas–target experiment: $v_0/c = 0.003$ ($\lambda_0 = 10.6\ \mu$m, $I_0 = 4.8\times 10^{11}$ W/cm^2), $v_e/c = 0.01$ ($T_e = 52$ eV), and $n/n_c = 0.01$ ($n_e = 10^{17}$ cm^{-3}). Then $2k_0\lambda_D = 0.2$ and $q = 17\epsilon$. The maximum homogeneous growth rate is $\gamma_0/\omega_0 = 10^{-3}$. Figure 1 shows the frequencies and growth rates of the three fastest growing modes $\omega_1, \omega_2, \omega_3$, as described in Sec. II, as functions of q. Figure 1(a) shows a weaker frequency dependence than anticipated from fluid theory. This is easily explained by the fact that damping reduces the coupling into neighboring modes, and hence larger q is required for a given frequency shift.

Figure 1(b) shows the same qualitative behavior as expected from fluid theory, with the γ of the mode ω_1 decreasing and that of the modes ω_2 and ω_3 increasing with increasing ripple amplitude. At large q, modes ω_1 and ω_2 were predicted to saturate at $\gamma = \gamma_0/\sqrt{2} \cong 0.67\omega_0$; in fact they sat-

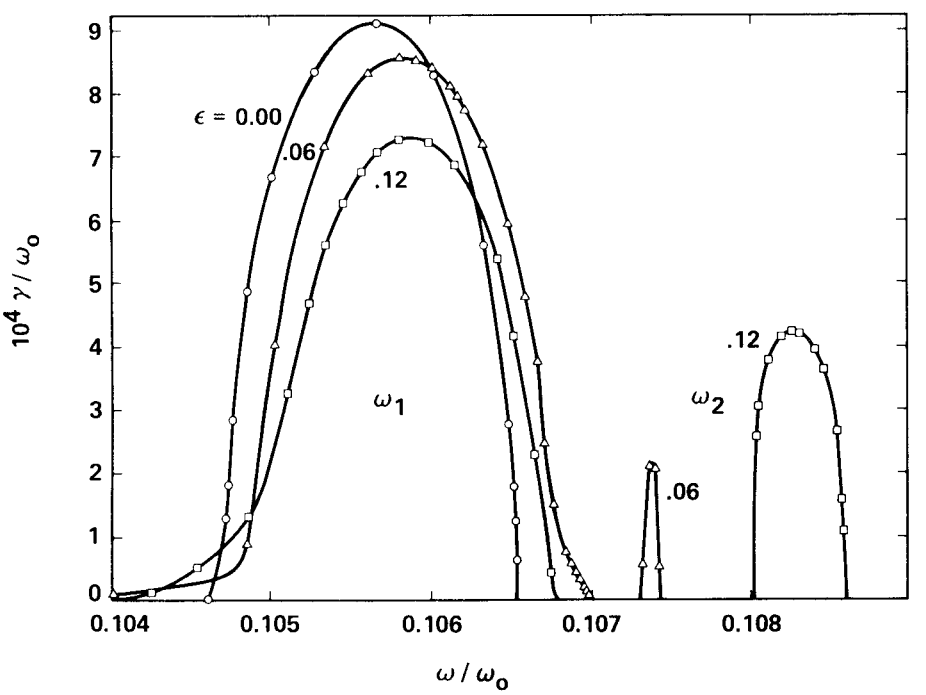

FIG. 2. Frequency "spectra" of the ω_1 and ω_2 modes for various ripple amplitudes ϵ.

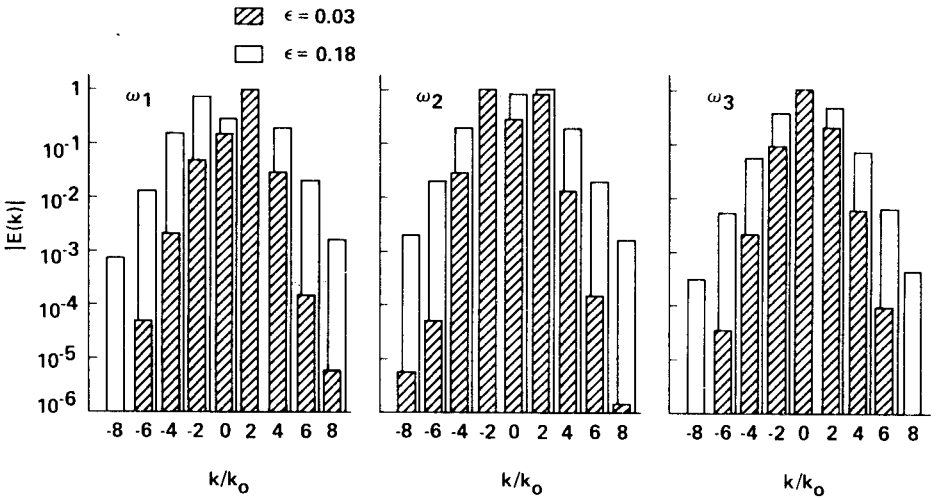

FIG. 3. The k spectra of the ω_1, ω_2, and ω_3 modes, computed for two values of the ripple amplitude ϵ.

urate at a lower level as a result of the inclusion of damping. The mode ω_3 is potentially the most dangerous. Not only does its fluid growth rate increase with q, but also its large phase velocity guarantees a very small level of Landau damping. We shall return to this mode later. Note that the phenomena shown here depend on q, and not on v_0/c. Increasing v_0/c would only change the scale of Fig. 1(b) by increasing γ_0. Though the range of q shown in Fig. 1 is unrealistically large for experiments where $\epsilon < 10\%$, this range was computed to bring out the asymptotic behavior and could actually be approached in experiments where nearly 100% Brillouin backscattering is seen.

Figure 2 is a more detailed plot of growth rate versus frequency for the ω_1 and ω_2 modes, showing how the ω_2 peak increases at the expense of the ω_1 peak as the ripple ϵ increases. Figure 3 shows the k spectrum of the ω_1, ω_2, and ω_3 modes for two ripple sizes. In fluid theory, one would substitute each eigenvalue of a into Eqs. (18)–(22) and solve for the Fourier components y_0, $y_{\pm 2}$, and $y_{\pm 4}$. The kinetic calculation of Fig. 3 did not require artificial truncation of the system; and the higher-k modes are naturally suppressed by Landau damping.

In Fig. 3, one sees that the original mode ω_1 has as its largest component the one usually associated with backscattering: $\kappa = 2$ or $k = 2k_0$. The ω_2 mode, however, is dominated by the $k = -2$ component, which has to be generated by mode coupling through the idler at $\kappa \cong 0$, *which has lower amplitude*. This strange behavior is explained in Sec. IV. The main component of the ω_3 mode is seen to be $\kappa \cong 0$, as expected. From Eq. (59) we see that, for small q, the effective value of $|k|$ is $k_0\delta$, which, from Eq. (17), is $|k| \cong \omega_p/c$. This means that the phase velocity is $\cong c$, as in forward Raman scattering; and electrons trapped and accelerated in this wave can give rise to a "superhot" distribution. The growth rate for forward Raman is $\gamma_F \cong (\omega_p/\omega_0)^{1/2}\gamma_0/2$. For the parameters of our calculation, γ_3 exceeds γ_F for $q > 0.67$, $\epsilon > 0.04$, which is easily achieved. The only difference is that the superhot electrons produced by the ω_3 mode, as it turns out, are in the $-\mathbf{k}_0$ direction, back toward the laser.

IV. WAVEFORMS AND PARTICLE ACCELERATION

In Sec. III, we found the amazing result that the new frequency ω_2, generated by mode coupling from the driven mode at $(\omega_1, 2k_0)$, has a k spectrum that is dominated not by the driven component at $k = 2k_0$ nor by the idler at $k \cong 0$ through which the energy must flow, but by a backward component at $k = -2k_0$. To understand why this is so, we first consider the nature of the normal Mathieu functions.

Figure 4(a) shows a plot of the function which, according to Eq. (30), describes the density perturbation of a plasma wave satisfying the rippled-plasma equation, Eq. (9):

$$y'' = -(a - 2q\cos 2z)y. \tag{73}$$

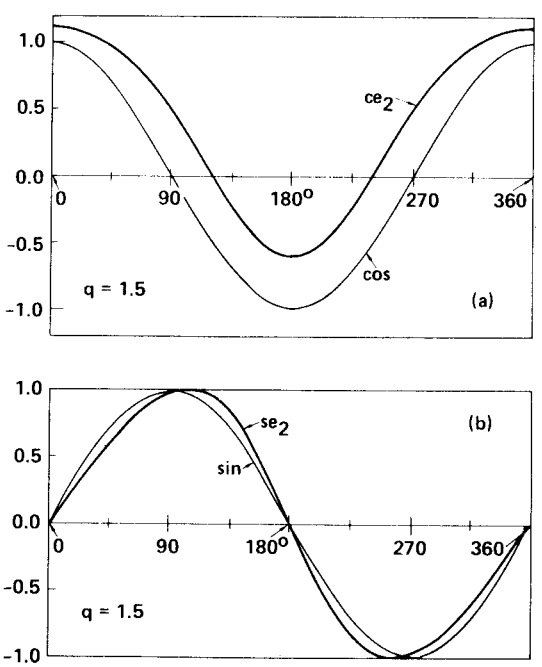

FIG. 4. Waveform of a resonant plasma wave in a rippled density $n_0(z)$ for (a) the even mode and (b) the odd mode, as compared with cosine and sine waves. The ripple follows the cosine curve.

In this case, the plasma wave has the same periodicity as the density ripple, which is also shown on Fig. 4(a). If q were 0, the curvature y'' would be $-ay$, as in a sine wave. The q term causes the curvature to be larger than usual where cos $2z$ is negative and smaller where cos $2z$ is positive. This causes the waveform to be flattened at the top and sharpened at the bottom. The result is that the amplitude is large over a large region near the peaks of $n_0(z)$, and is large over only a small part of the region near the troughs of $n_0(z)$. Consequently, the average ω_p "seen" by the perturbation is larger than in a uniform plasma. This gives the mode a frequency [Eq. (30)] higher than the Bohm–Gross frequency for zero ripple. Similarly, Fig. 4(b) shows the odd mode se_2, which has its curvature modified by Eq. (73) in such a way that the skewed sine wave has large amplitude near the minima of $n_0(z)$. Thus the frequency of this mode [(Eq. 29)] is lower than for $q = 0$. These waveforms can be decomposed into spatial harmonics which are phase locked to each other and to the ripple.

Now when the plasma wave has a slightly different wavelength than the ripple, it would appear that the wave cannot be phase locked to the ripple, and that therefore the wave must, on the average, feel the average density. To show that this is not necessarily so, consider the harmonics y_0, $y_{\pm 2}$, and $y_{\pm 4}$ as given by the truncated set, Eqs. (23) and (24). Defining

$$\beta_{\pm} = y_{-2}/y_2 = [1 \pm (1+R^2)^{1/2}]/R, \tag{74}$$

we see that β_+ corresponds to the higher frequency wave ω_2 and β_- to the lower frequency wave ω_1. In terms of β, Eqs. (23), (26), and (27) give

$$\frac{y_0}{y_2} = \frac{q}{4}(1+\beta), \quad \frac{y_4}{y_2} = -\frac{q}{12}, \quad \frac{y_{-4}}{y_2} = -\frac{q}{12}\beta. \tag{75}$$

The y_2 component has $\kappa = 2 - \delta$, and therefore it varies as $\exp i[(2-\delta)z - \omega t]$. The other components have arguments differing by exactly $\pm 2z$. We normalize to $y_2 = 1$ and define

$$\theta = \omega t + \delta z. \tag{76}$$

Adding the components together according to Eqs. (74) and (75) and taking the real part, we obtain

$$y = \cos(\theta - 2z) + \beta\cos(\theta + 2z) + (q/4)(1+\beta)\cos\theta - (q/12)\cos(\theta - 4z) - (q/12)\beta\cos(\theta + 4z). \tag{77}$$

For our purposes here it will be sufficient to keep only the first three terms. From Eq. (74), we see that, when R is small, β_+ is $\gg 1$ while β_- is $\ll 1$. Separating out the standing wave component in Eq. (77) according to the size of β, we obtain for the two modes

$$(\omega_1): \; y \cong \underset{(1)}{(1-\beta_-)\cos(\theta - 2z)} + \underset{(2)}{[2\beta_-\cos 2z} + \underset{(3)}{(q/4)(1+\beta_-)}]\cos\theta, \tag{78}$$

$$(\omega_2): \; y \cong \underset{(1)}{(\beta_+ - 1)\cos(\theta + 2z)} + \underset{(2)}{[2\cos 2z} + \underset{(3)}{(q/4)(1+\beta_+)}]\cos\theta. \tag{79}$$

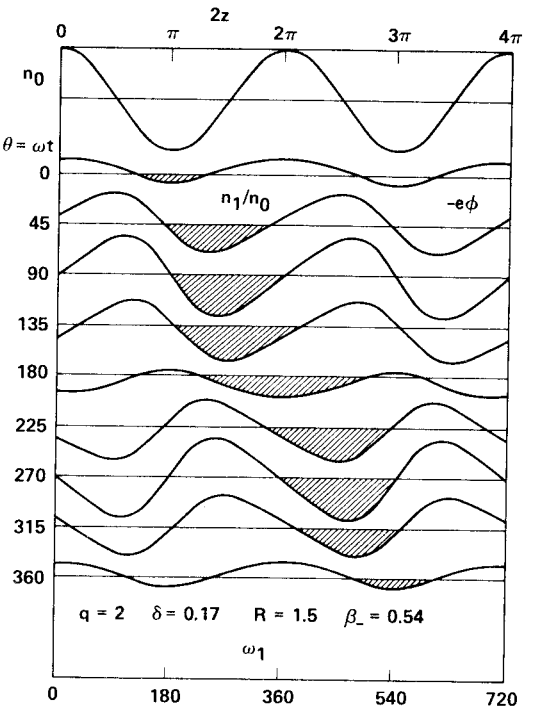

FIG. 5. Waveform of $n_0(z)$ and the low-frequency plasma wave ω_1 in the nearly resonant case. The value of q has been exaggerated (see the text).

We see that each wave has (1) a traveling wave component, (2) a standing wave component, and (3) a time-varying base line shift which changes only slowly with z as a result of the term δz in θ.

Equation (77) for the ω_1 and ω_2 modes is plotted in Figs. 5 and 6, respectively, together with the ripple $n_0(z)$, over two cycles in the phase $2z$ and one cycle in the phase

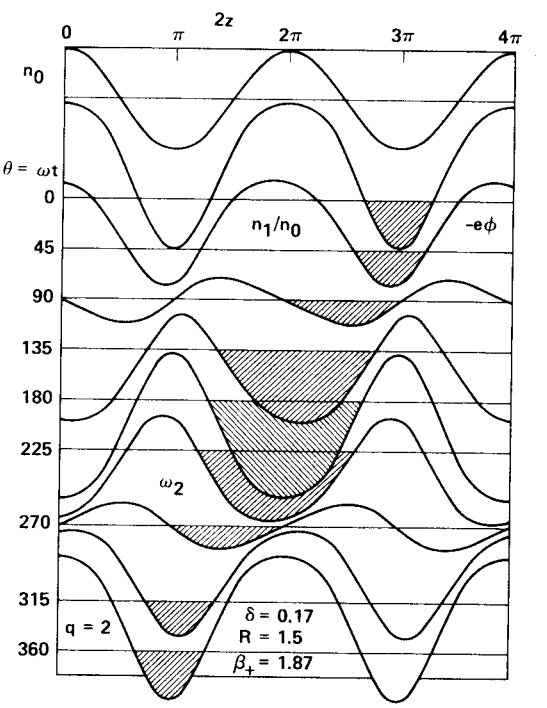

FIG. 6. Same as Fig. 5, but for the high-frequency wave ω_2.

$\theta \cong \omega t$. For clarity, the large value $q = 2$ was chosen; but the formulas are based on small q, and the actual waveforms for $q = 2$ will be somewhat different. In Fig. 5, we see a traveling wave moving to the right, as predicted by the term (1) in Eq. (78). The $y_{\pm 4}$ components cause the waveform to be distorted and the peaks to move nonuniformily to the right. Since the ripple is nonresonant, the wave peaks must pass regions where n_0 is large as well as where it is small. However, the standing wave component of term (2) in Eq. (78) causes the total wave amplitude to be small whenever the wave maximum or minimum passes the peaks in n_0. Thus, the average density seen by the wave is lower than usual, and ω_1^2 is less than $\omega_{p0}^2 + 3k^2 v_e^2$. The base line shift, term (3) in Eq. (78), can be seen in Fig. 5 but does not play a large role in the frequency reduction.

For the ω_2 mode, the average density seen by the wave must be higher than normal. The way this is accomplished is shown in Fig. 6. There is a backward traveling wave, corresponding to term (1) in Eq. (79), and a standing wave, term (2), causing the entire wave to have a small amplitude at $\theta \cong 90°$ and 270°. However, the dominant effect here is the base line shift, term (3), which ensures that the wave amplitude is large whenever the maximum or minimum of n_1/n_0 passes the peaks in n_0. This causes a larger than normal effective ω_p.

The base line shift actually changes in space as a result of the δz term in θ. To see this, we need only to repeat the patterns of Fig. 6 over distances z of order $1/\delta$, advancing the value of θ with ωt constant. Such a waveform is shown in Fig. 7. The envelope of potential oscillations is seen to have deep minima, which could be called "superwells." Particle acceleration can be seen from the potential wells shown shaded in Figs. 5 and 6. The low-frequency mode ω_1 traps electrons and accelerates them forward, in the direction $\mathbf{k}_0$. The high-frequency mode, on the other hand, accelerates electrons backward, in the direction of $-\mathbf{k}_0$. Electrons trapped in this mode, however, can be detrapped by the slow change in the wave envelope, as shown in Fig. 7. Those that are spilled out can still be trapped in the superwell formed by the envelope. The superwell travels with a velocity $\omega_p/k \cong c$ in the *backward direction* and can give rise to superhot electrons traveling opposite to $\mathbf{k}_0$. The injection of electrons of sufficient energy to be trapped by the fast-moving superwell can be accomplished by preliminary acceleration in the slow-moving individual potential wells.

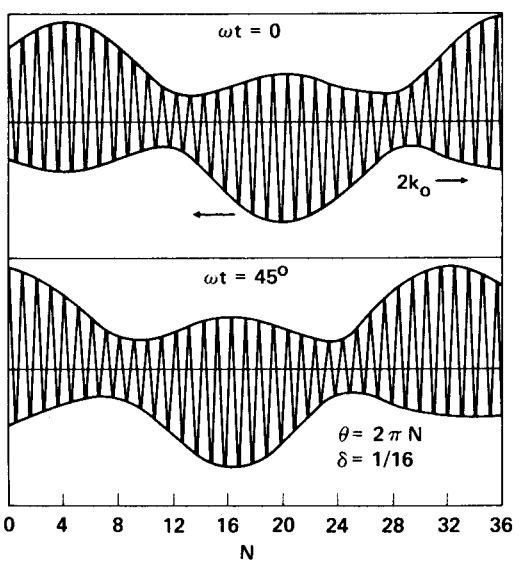

FIG. 7. Waveform of the mode ω_2 over a k-mismatch distance.

The relation among the Fourier components y_0, $y_{\pm 2}$, and $y_{\pm 4}$ is therefore rigorously determined by the need to generate traveling waves, standing waves, and baseline shifts in the right proportion to allow the wave to "see" smaller or larger than average density, thus causing the frequency splitting to ω_1 and ω_2. In particular, the mode ω_2 must have a large component $\mathbf{k} \cong -2\mathbf{k}_0$ in order to achieve its high frequency. It does not matter which k component of ω_2 is excited; the k spectrum for the eigenmode is determined by the k mismatch.

From Fig. 7 it is clear that the wave has two periodicities, one with $|k| \cong (2 - \delta)k_0$ and the other with $|k| \cong \delta k_0$. The beat between these satisfies the Floquet condition that a solution of Eq. (9) must be of the form $y = e^{ivz}P(z)$, where $P(z)$ has period π. Specifically, we can rewrite Eq. (77) as

$$y = Y(z)e^{i\phi(z)} \cos[\omega t - (2 - \delta)z], \tag{80}$$

where

$$Y(z) = D \sec \phi, \tag{81}$$

$$\tan \phi = N/D, \tag{82}$$

$$N = \left(\frac{q}{4}(1 + \beta) + \frac{q}{12}\right)\sin 2z + \beta \sin 4z - \frac{q}{12}\beta \sin 6z, \tag{83}$$

$$D = 1 + \left(\frac{q}{4}(1 + \beta) - \frac{q}{12}\right)\cos 2z + \beta \cos 4z - \frac{q}{12}\beta \cos 6z. \tag{84}$$

It is clear that $P(z) = Y(z)e^{i\phi(z)}$ has period π.

Finally, the nature of the mode ω_3 can be seen from Eqs. (55) and (56), which give

$$y_0/y_2 = -4/q, \quad y_{-2}/y_2 = 1. \tag{85}$$

Thus, the mode consists of a standing wave and a large baseline shift, which combine to cause the wave amplitude to be large where n_0 is small. Thus ω_3 falls below ω_{p0}. The baseline shift is actually a long wavelength mode with $k = -\delta k_0 \cong -\omega_p/c$, and as such can accelerate superhot electrons in the backward direction. Since all three modes discussed here can occur simultaneously, we emphasize again that preacceleration in one of the slow waves can cause electrons to be more easily trapped in a fast-moving potential well.

V. SUMMARY

We have examined the excitation of plasma waves in a rippled density profile, paying special attention to the case arising in simultaneous Brillouin and Raman scattering where the ripple has a slightly shorter wavelength than the plasma waves. The problem is treated kinetically so that the infinite series of harmonics that arises from mode coupling is naturally truncated by Landau damping. The physical pro-

cesses are made clear by a detailed fluid treatment, which shows that the usual SRS growth rate is reduced by the ripple, but that energy now goes into exciting two new modes. Kinetic calculations give the frequencies, growth rates, and k spectra of the three dominant modes for different ripple sizes. The new modes are found to propagate primarily in the opposite direction to the originally excited plasma wave. A study of the waveforms clarifies the physical reasons for this. Electrons trapped in these waves can be accelerated, either undesirably, as in laser fusion, or purposefully, as in plasma accelerators. The ripple causes electron acceleration to occur in both forward and backward directions, and in addition can produce electrons in the backward direction of the same ultrahigh energy as is associated with forward Raman scattering.

ACKNOWLEDGMENTS

Since our work was initially reported,[17] several other papers have appeared on this subject. C. Darrow[18] has computed the importance of mode coupling as a saturation mechanism in beat-wave excitation of plasma waves. Figueroa and Joshi[19] have used the frequency splitting discussed here to explain the double peak in half-harmonic radiation. Rozmus *et al.*[20] have computed the interaction of SRS and SBS using the Zakharov equations. Aldrich *et al.*[21] have found from computer simulations that ion waves can trigger the collapse of the plasma waves, profoundly changing the nature of SRS. We thank these colleagues for their interest and acknowledge interesting discussions with them.

This work was supported by the U. S. Department of Energy, Contract DE-AS08-81-DP40166 and the National Science Foundation, Grant No. ECS83-10972. One of us (HCB) wishes to thank the other of us (FFC) for his hospitality at UCLA during the analysis stage, and the Los Alamos Scientific Laboratory for hospitality during the computational state of this work.

[1]W. L. Kruer, K. Estabrook, B. F. Lasinski, and A. B. Langdon, Phys. Fluids **23**, 1326 (1980); **26**, 1892 (1983).
[2]D. W. Phillion, D. L. Banner, E. M. Campbell, R. E. Turner, and K. G. Estabrook, Phys. Fluids **25**, 1434 (1982).
[3]W. Seka, E. A. Williams, R. S. Craxton, L. M. Goldman, R. W. Short, and K. Tanaka, Phys. Fluids **27**, 2181 (1984).
[4]R. G. Watt, R. D. Brooks, and Z. A. Pietrzyk, Phys. Rev. Lett. **41**, 170 (1978).
[5]A. A. Offenberger, R. Fedosejevs, W. Tighe, and W. Rozmus, Phys. Rev. Lett. **49**, 371 (1982).
[6]H. Figueroa, C. Joshi, and C. E. Clayton, Phys. Fluids **30**, 586 (1987).
[7]C. Joshi, W. Mori, T. Katsouleas, J. M. Dawson, J. M. Kindel, and D. W. Forslund, Nature **311**, 525 (1984).
[8]C. E. Clayton, C. Joshi, C. Darrow, and D. Umstadter, Phys. Rev. Lett. **54**, 2343 (1985).
[9]B. Amini and F. F. Chen, Phys. Fluids **29**, 3864 (1986).
[10]G. R. Mitchel, T. W. Johnston, and H. Pépin, Phys. Fluids **27**, 1527 (1984).
[11]P. K. Kaw, A. T. Lin, and J. M. Dawson, Phys. Fluids **16**, 1967 (1973).
[12]D. R. Nicholson, Phys. Fluids **19**, 889 (1976).
[13]W. Rozmus, A. A. Offenberger, and R. Fedosejevs, Phys. Fluids **26**, 1071 (1983).
[14]C. S. Liu, M. N. Rosenbluth, and R. B. White, Phys. Fluids **17**, 1211 (1974).
[15]M. Abramowitz and I. A. Stegun, *Handbook of Mathematical Functions* (Dover, New York, 1965), p. 721ff.
[16]B. D. Fried and S. Conte, *The Plasma Dispersion Function* (Academic, New York, 1961).
[17]H. C. Barr and F. F. Chen, in *1982 Anomalous Absorption Conference*, Santa Fe (Los Alamos National Laboratory, Los Alamos, NM, 1982), Paper B-13; F. F. Chen and H. C. Barr, in *1984 Anomalous Absorption Conference*, Charlottesville, VA (Naval Research Laboratory, Washington, D.C., 1984), Paper B-5; F. F. Chen, C. Joshi, C. E. Clayton, B. Amini, and H. C. Barr, in *Proceedings of the Japan–U.S. Seminar on Theory and Application of Multiply Ionized Plasmas Produced by Laser and Particle Beams*, Nara, Japan, 1982 (Institute of Laser Engineering, Osaka University, Osaka, Suita, Japan), p. 243.
[18]C. Darrow, D. Umstadter, T. Katsouleas, W. B. Mori, C. E. Clayton, and C. Joshi, Phys. Rev. Lett. **56**, 2629 (1986); C. Darrow, Ph.D. thesis, University of California, Los Angeles, 1986.
[19]H. Figueroa and C. Joshi, submitted to Phys. Fluids.
[20]W. Rozmus, J. Samson, R. P. Sharma, W. Tighe, and A. A. Offenberger (private communication).
[21]C. H. Aldrich, B. Bezzerides, P. F. Du Bois, and H. A. Rose, Comments Plasma Phys. Controlled Fusion **10**, 1 (1986).